In-situ damage detection in SMA reinforced CFRP

F. Pinto, F.Ciampa, U. Polimeno, M. Meo

Material Research Centre, Department of Mechanical Engineering,

University of Bath, Bath, UK

Abstract

The purpose of this paper is to analyse the possibility to manufacture and verify the self-sensing capability of composite materials plates with an embedded network of NiTi shape memory alloys (SMA) used as transducers for structural integrity. Firstly, the thermo-electrical material properties of SMAs were investigated to assess their capability to sense strain within. The results showed that the electrical resistance variation provided by the shape memory alloys network enables a built in and fast assessment of the stress distribution over the entire structure. Then, by transmitting a low amperage current, results in an electric and thermal flow through the entire SMA network. Using an IR Camera it is possible to capture the emitted thermal waves from the sample and create an image of the thermal field within the material. Consequently, analysing the behaviour of the heating curves on different points of the sample, it is possible to identify potential variation in the apparent temperature of the composite, leading to the identification of damages within the composite structure.

Keywords: Shape Memory Alloys, damage detection, emitted thermal energy, thermal diffusivity

1. Introduction

The possibility to develop materials that can be tailored to various structural needs has led to an increased use of carbon fibre-reinforced composites (*CFRP*) for those applications which require high mechanical properties and very low weight, such as aerospace and automotive sector.

However, one of the major drawbacks of composite materials is that they can be seriously damaged from impact of foreign objects, leading to various types of damages such as microcracks, delamination and barely visible impact damages (*BVID*). Mechanical properties of the part can be severely affected by the presence of these localised impact damages, which can result in dramatic failures. Although several authors have studied the behaviour of composite structures when subjected to impact [1-4], the possibility of monitoring the structural integrity of key parts is still an issue because of the intrinsic complexity of composite materials and the need to further improve the safety of structures. Several Non Destructive Evaluation (*NDE*) techniques such as shearography [5], thermography, eddy current and radiography are used to inspect the integrity of a part, however most of them require that all parts have to be taken out from the structure and to be analysed separately, resulting in time consuming and expensive procedures [6]. To solve this problem, the past decade has seen the rapid development of Structural Health Monitoring systems, which imply the integration of NDE methods in a material in order to enable autonomous state awareness for structural integrity. A new-generation materials is being developed characterised by an embedded complex sensor-based network integrating signal analysis and transmission capabilities, resulting in a *smart* material able to provide information about the integrity of structural components. The sensors network can be obtained exploiting peculiar properties of specific materials, such as piezoelectric components [7], carbon nanotubes [8], optical fibres [9] and Micro-Electro-Mechanical

Systems (*MEMS*) [10]. Shape Memory Alloys (*SMA*) are novel materials with the unique ability to recover their initial shape after a solicitation and they have been studied as a possible reinforcement media to improve impact resistance and damping properties of composite panels [11-14]. Moreover, because of their *electro-thermal* properties, these new generation materials can be exploited as sensors and actuator for SHM in composite parts [15]. Hence, unlike other smart materials, SMA-reinforced CFRP are simultaneously structural, functional and *smart* materials, due to their high mechanical properties, high thermal and electrical conductivity and SHM properties. This work is focused on the characterisation of a new multifunctional material, obtained embedding SMA wires within traditional carbon fibres reinforced epoxy composites. The multifunctionality of the material lies in the possibility to use SMA not only to increase impact resistance but also, exploiting their intrinsic properties, to create a network of sensors that can be employed for SHM and NDT.

2. Material and Methods

2.1. SMA Overview

The particular properties of a SMA rise from the presence of two different crystalline phases within its structure [16]: the *martensitic phase* (*M*) and the *austenitic phase* (*A*). The martensitic phase is stable below a specific value of temperature called *martensite finish transformation temperature* (*Mf*), while the austenitic phase is stable above the *austenite finish transformation temperature* (*Af*), with Af>Mf (*Figure 1*). The peculiar properties of SMA are the result of the thermoelastic phase transition between austenite and martensite. This mechanism is defined as diffusionless as it does not involve chemical modification of the material but only a rearrangement of the crystalline structure at the lower energy configuration for a given temperature. Indeed, each phase is characterised by a specific crystalline structure, i.e. martensite is arranged in a tetragonal body centred configuration and austenite presents a face centred cubic structure.

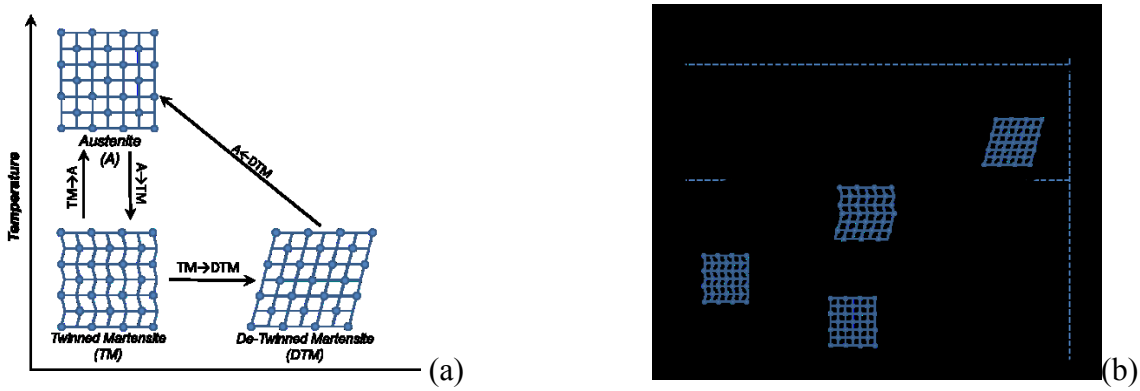

Figure 1- a) Different phase transitions for SMA; b) shape memory effect

Due to the high symmetry of austenite, when a single austenitic crystal is cooled below *Mf*, the martensite phase can assume multiple configurations, called variants. Therefore, two different typology of martensite can be distinguished: stress-free martensite, characterised by a multi-variant twinned configuration (*TM*) and stress-induced martensite, characterised by a detwinned configuration (*DTM*). The difference between these two configurations relies in the different response to an external deformation. Indeed, while stress-free martensite can minimise only the effect of small local deformation, stress-induced martensite is able to withstand higher macroscopic

deformations due to the alignment of all the variants. As it is possible to observe from *Figure 1*, for temperatures below *Mf* the material is in its fully martensitic phase, hence, applying a stress it is possible to observe an initial elastic deformation (A) followed from the transformation from multivariant to single-variant martensite (B) once a critical stress value is reached. When the external stress is removed an elastic recovery takes palace (C). At this point, when the temperature is increased above Af, the phase transformation between de-twinned martensite and austenite is activated (D), resulting in a full recovery of the initial shape.

2.2. Samples Manufacturing

In order to analyse the SHM ability of SMA-reinforced composites, several samples were manufactured, embedding NiTi SMA wires with a diameter of 350μm (*Figure 2*) within laminates obtained with different lay-up sequence. The prepreg used was a M21 carbon fibres prepreg. All the samples were prepared via manual stratification and hot press curing at 180ºC for 2 hours.

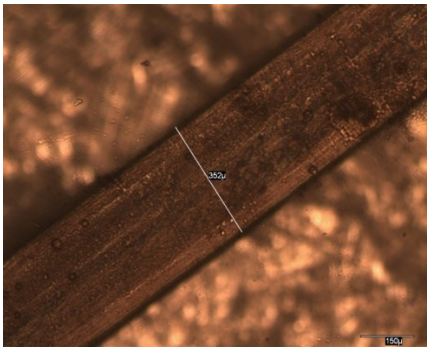

Figure 2 - Optical microscope image of a single NiTi wire

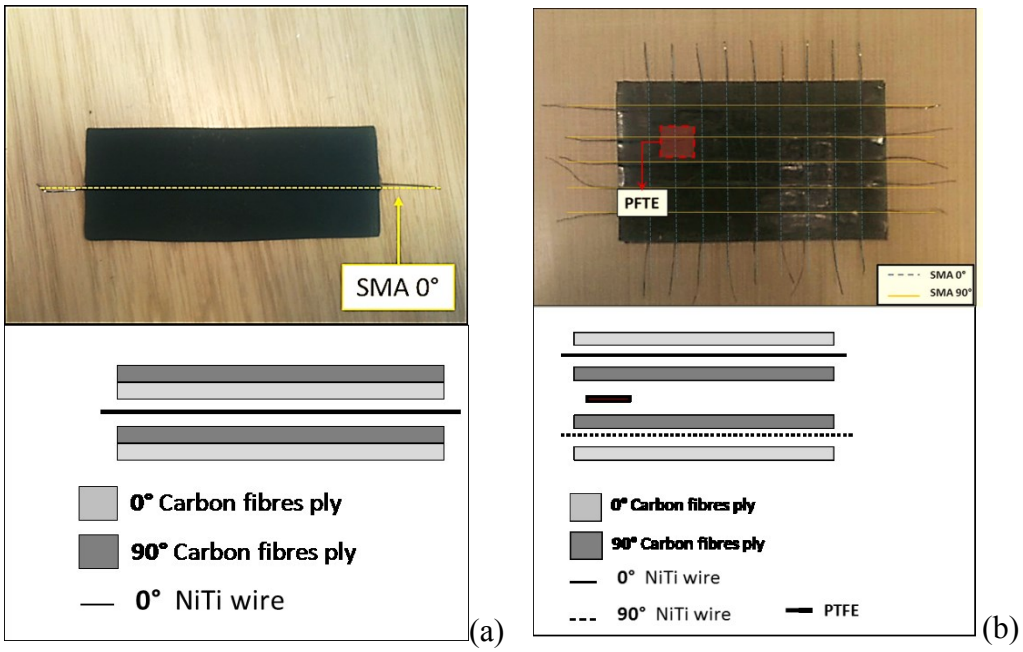

Figure 3 - a) single NiTi embedded CFRP sample; b) multiple NiTi embedded CFRP sample with single PFTE patch (4 layers)

In order to test the thermo-electrical behaviour of the SMA composites, a first sample was obtained

embedding a single NiTi wire within a 4 layers laminate, labelled as *Sample A* (*Figure 3a*).
Afterwards, a different sample design was developed in order to test the sensitivity of the SHM system (*Sample B*). This layout counts two different series of NiTi disposed at 0º and 90º in order to form a SMA sensors grid with an inter-wire distance of 10 mm. The wires were embedded within a laminate with the stack sequence shown in *Figure 3b.* In order to simulate the presence of a damage a patch of PTFE was inserted in the middle plane of the sample.
The last sample, labelled *Sample C*, was prepared in such a way to embed multiple damages in a thicker plate. The laminate was obtained with 16 plies and three different PFTE patches were layered at different depth (1.25, 1 and 0.575 mm for the top surface). The orthogonal SMA network was included in the sample with the same inter-wires distance of the previous sample (*Figure 4*).

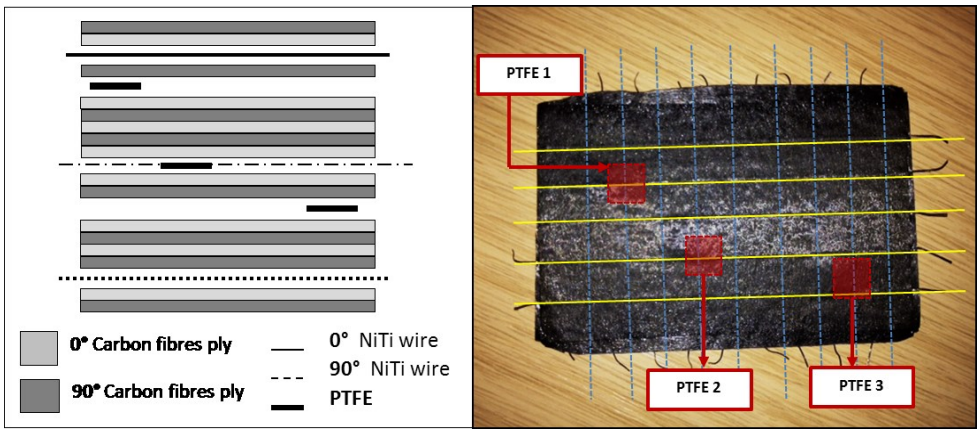

Figure 4 - NiTi network embedded CFRP sample with multiple PFTE patches (16 layers)

3. Strain Sensing

The capability of using SMA as sensors for real time monitoring of strain distribution was studied, exploiting the variation of particular properties of the material. Indeed, being able to measure such variations, it is possible to control when a structural key point of a part is undergone to tensile or compressive strength above a certain critical value.

3.1. Strain Sensing Results and discussion

Results obtained from Cui et al [17] have shown that there is a relationship between the strain and the electrical resistance variation of SMA wires. However, such a relationship is linear and temperature independent only when the material is in its fully martensite phase, whilst for the austenitic phase it becomes more complicated. Therefore, temperature during all the tests was set in order to be always below Mf. The sensing ability of SMA wires were first tested by loading a single NiTi wire (R_0=2.5 Ω) in a tensile machine and measuring the resistance variation with a 6-digit precision multimeter (*Figure 5a*). As it is possible to observe from *Figure 5b*, after an initial elastic deformation, the stress-strain curve of NiTi wires exhibits the typical SMA plateau, which corresponds to the de-twinning of martensite. However, during the martensite phase transformation, the variation of the electrical resistance still increases almost linearly with the strain, confirming the

sensing ability of NiTi wires [11]. Nevertheless, an impact event is characterised by a very different stress distribution in comparison with a pure tensile loading. Indeed, while during the tensile test the SMA wires are loaded only in the longitudinal direction, during an impact the material is stressed also in the out of plane direction and under compressive stresses. As a consequence, in order to investigate the sensitivity of SMA-based composites, flexural tests were carried on *Sample A* in three-point-bending mode (*Figure 6a*). *Figure 6b* represents the results from the flexural test showing that the electrical resistance variation remains linear with the increase of the flexural extension. As a result, monitoring the dynamic behaviour of electrical resistance is it possible to analyse the strain distribution within the composite part.

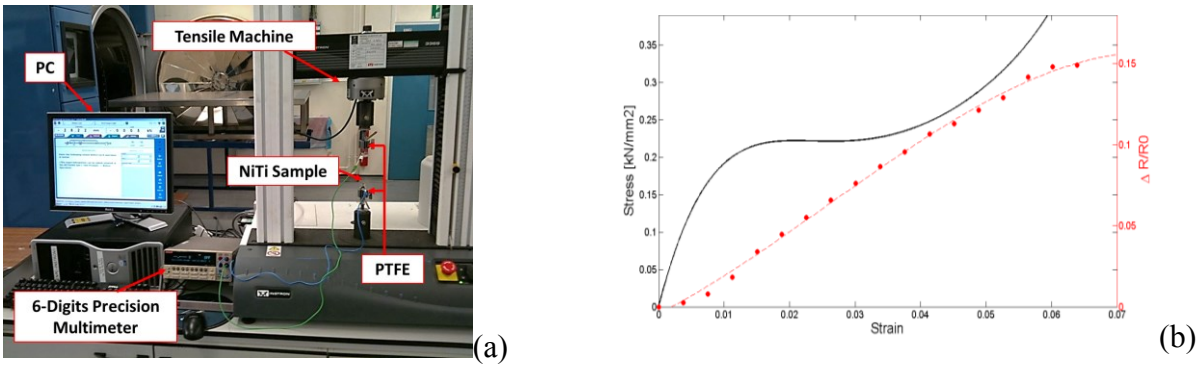

(Figure 5 – a) Experimental setup; b) Stress-Strain behaviour and electrical resistance variation of NiTi wires in tensile mode

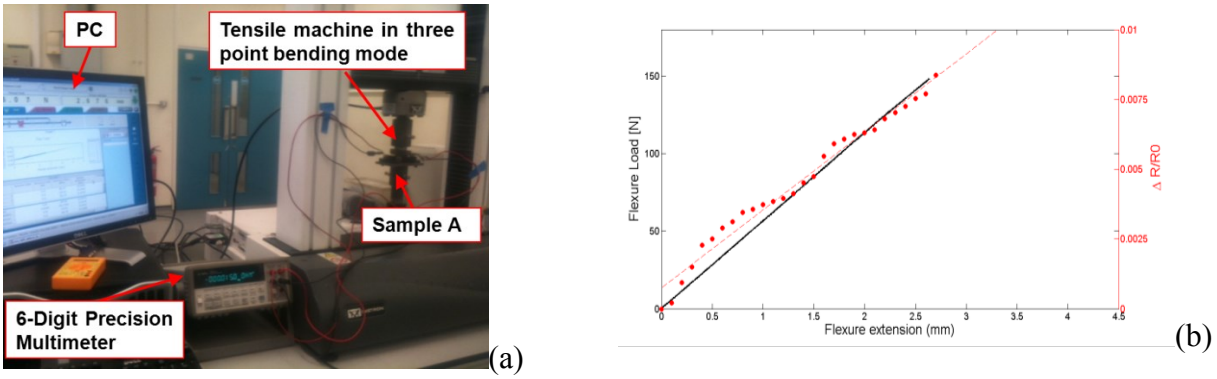

Figure 6 – a) Experimental setup; b) Flexural Load versus Flexural Extension and electrical resistance variation for SMA-based composites

4. Thermography

Active Infrared Thermography (IT) is based on the analysis of the temperature gradients responses at the medium surface due to heat stimulation. Data are recorded using an infrared camera (IR) and can give information about the integrity status of structural components. These thermal responses can identify the internal state of the material due to the difference in the heat diffusion rate that rises when the thermal waves flow by diffusion on a damaged part [18]. IT can be performed using different approaches, depending on how the thermal waves are generated and the most common techniques are lock-in, pulsed and step heating thermography [19, 20]. Lock-in thermography (LT)

employs a periodic heat excitation to achieve information on the structural damage, by using the reflected and incident thermal waves magnitude or phase. However, as the probing depth is determined by the excitation frequency, LT is time consuming for defects located at various depths in the test specimen, and requires sophisticated data acquisition systems to input the heat source. In pulsed thermography (PT), a short duration energy pulse is applied and the specimen subsurface structure is revealed through the surface temperature evolution. Nevertheless, this approach is not suitable for thick and low conductive materials, as the intensity of the pulse is limited to avoid damaging the structure. Unlike PT, in step-heating thermography (SHT) a low intensity pulse (heat source) is applied for a long period, thus enabling a longer heating time to locate deeper defects. However, one of the major drawbacks of all these approaches is that they all need an external heat source such as high-power flashes or infrared radiators [21], leading to expensive and time-consuming techniques that cannot be employed for in situ assessment of the defects. The use of the composite parts reinforced with SMA can overcome this issue using the NiTi network wires as an internal heat source to generate an in situ low power resistive heating (Joule effect), resulting in a *built in* SHM system for composite structures.

4.1. Experimental Set-up

As it is possible to observe from *Figure 7a*, the samples were heated by applying on the NiTi network a long pulse of electric current at constant amplitude of 1 A. Current was provided using a power supply and an electrically cooled Infra-red Camera (CEDIP) was used to acquire the thermal images.

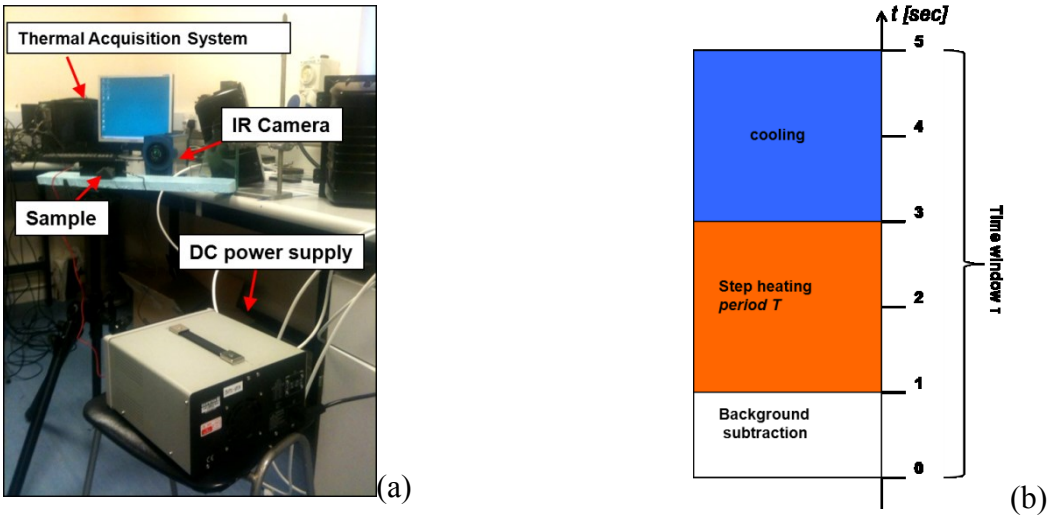

(Figure 7 - a) Experimental Setup; b) observation time of the IR camera in the step-heating process

The resolution of the camera was 320x240, while temperature sensitivity and maximum frame rate were 30 mK and 150 Hz respectively. In order to analyse the temperature evolution during and after the heating process, SHT was chosen as active thermography method for the evaluation of the apparent temperature at the test piece surface. Thermal images were acquired with an interval of 0.01 sec for a total observation time (τ) of 5 sec. To overcome the effects given by imperfect heating or

heat noise, a background subtraction was carried out on the first 100 frames (1 sec) of acquisition, computing the average for every pixel of the IR camera (*Figure 7b*). In the following images units of temperature will not be reported because the surface temperature is proportional to the camera's digital level output .However, the same scale is used for all tests carried out.

4.2. Thermography Results and Discussion

Tests conducted on *Sample B* are shown in *Figure 8* and *9* and they represent the thermograms measured at the end of the step-heat excitation (t=3 sec). Epoxy resin within the CFRP is characterised by a low thermal diffusivity, thus the heat generated via Joule effect in the NiTi wires does not spread immediately but it is initially confined only in the area surrounding the SMA. This is clearly shown in *Figure 8a* and *8b*, which represent the thermal response of the composite when the current flows on a vertically and horizontally aligned NiTi wire through undamaged areas. As it is possible to notice from the images, the variation in apparent temperature changes uniformly all over the area in which the current is flowing, while the rest of the sample is not affected.

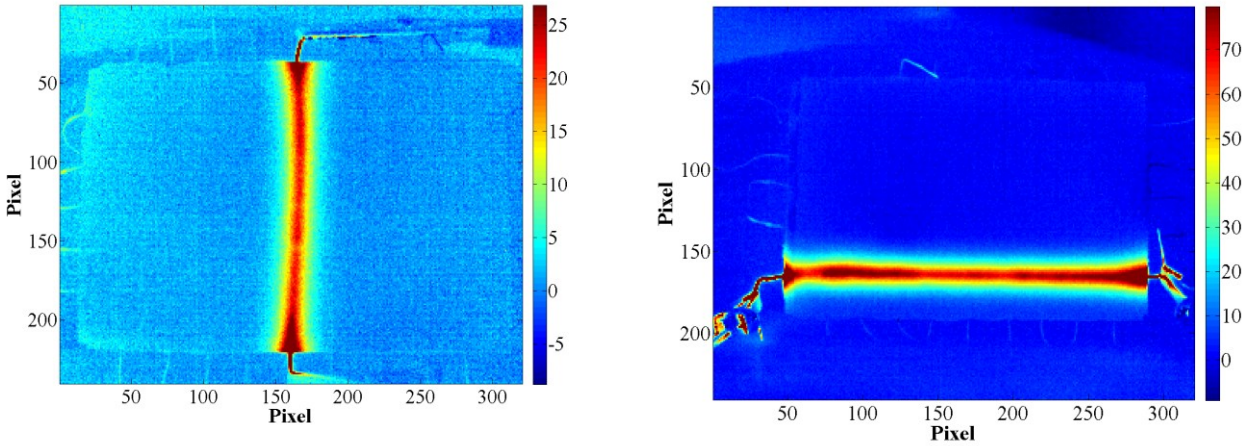

Figure 8 - Thermography images for undefective parts of sample B at t=3s

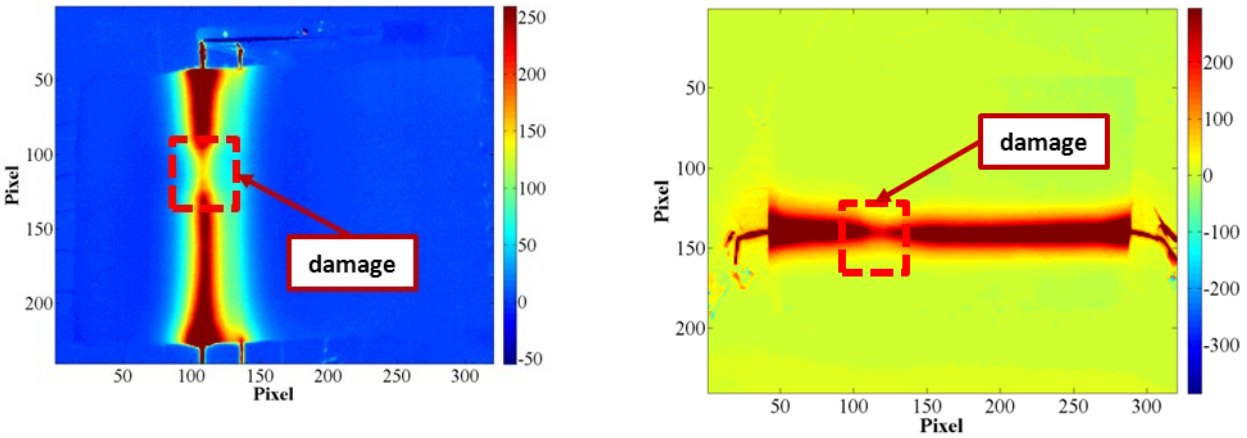

Figure 9 - Thermography images for defective parts of sample B at t=3s

Images 9a and *9b* represent instead the thermal response of the composite when damaged parts are

analysed. Indeed, the presence of damage within the thickness is immediately identified by a large variation in the apparent temperature of the sample. This effect is generated because the heat flow, due to Joule heating, is impeded by the increase of thermal resistance (PTFE patch) around the damaged area. In other words, the diffusion rate at that specific point is reduced by the presence of a subsurface discontinuity, resulting in a recorded apparent temperature variation on the surface. Information regarding the structural integrity of the sample can be also investigated by analysing the time history of the apparent temperature for the pixels associated to a non-defective area in comparison with those from a defective area. *Figure 10* represents the behaviour of the observed temperature during the entire test for a damaged (continuous curve) and an un-damaged point (dashed curve).

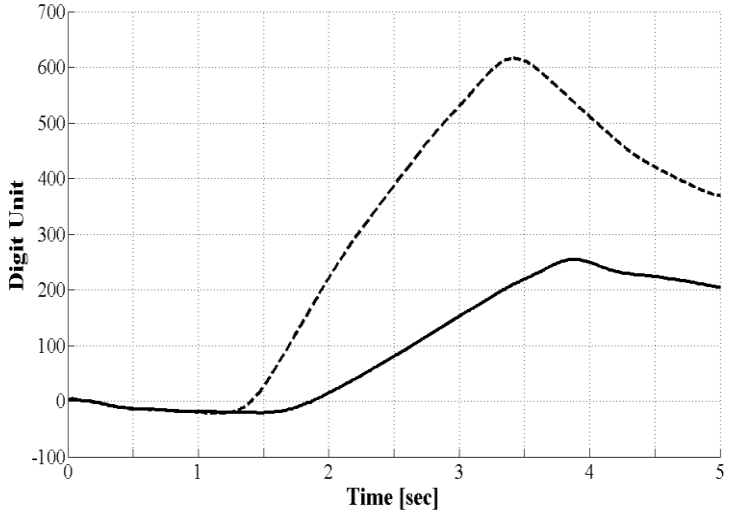

Figure 10 - Apparent temperature variation over time for damaged and undamaged areas

Analysing the curves it is possible to observe that the presence of the damage has several effects on apparent temperature over time. Indeed, not only the peak of apparent temperature is lower for a damaged part in comparison with an un-damaged one (which is the effect seen in the thermograms), but also both heating and cooling rates are affected by the PFTE discontinuity. Another important results obtained with this technique is the possibility to assess the severity of a detected damage with high spatial resolution (even below the inter-wire distance). Indeed, by simply recording the thermal waves after heating two NiTi wires surrounding the damage and then looking at the high apparent temperature variation around the PTFE patch, it is possible to obtain a qualitative image of the defect size (*Figure 11*). By means of a simple calibration obtained with *a priori* knowledge of the inter-wire distance and the length of the SMA wires, a rough estimation of the size of the internal damage was provided (approximately 10 mm length and 10 mm width).
Further tests were conducted on *Sample C*, in order to analyse the behaviour of the SMA-based composite when multiple damages are located within the thickness. *Figure 12* represents the results for the experiments carried out on the multi-damaged sample. A current of 1A was driven in two different NiTi wires using a two-channel power supply, in order to analyse the sensitivity of the technique with damages far from the top surface. As it is depicted in *Figure 12a*, the technique provides remarkable results also for damages that are located deeper within the sample. Indeed, the

positions of *PTFE3* (positioned at 1.25 mm from the surface) and *PFTE1* (positioned at 0.575 mm from the surface) are immediately detected by the IR-camera as the apparent temperature shows large variations for both discontinuities. Signals acquired from the camera were analysed separately and a contrast observed temperature analysis was carried out in order to evaluate only the effect given by the damages, according to the following equation:

$$C_{A_i} = \|A_{und_i} - A_{dam_i}\|$$

where C_{Ai} is the contrast signal, A_{undi} is the signal recorded for a undamaged part on the *i*th wire and A_{dami} is the signal recorder for a damaged point on the same *i*th wire. Results in *Figure 12b* show a slight decrease of the apparent temperature peak for PFTE3 in comparison with PFTE1.

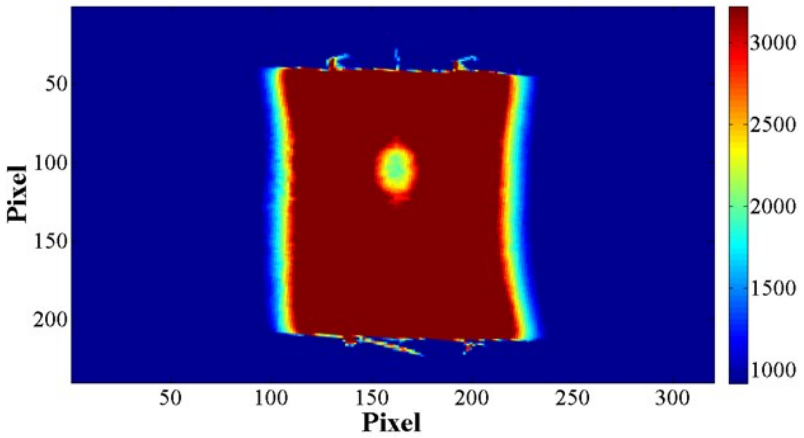

Figure 11 - Thermal image of the apparent temperature for sample A obtained at t=3 sec with double vertically aligned NiTi wires surrounding the PFTE patch

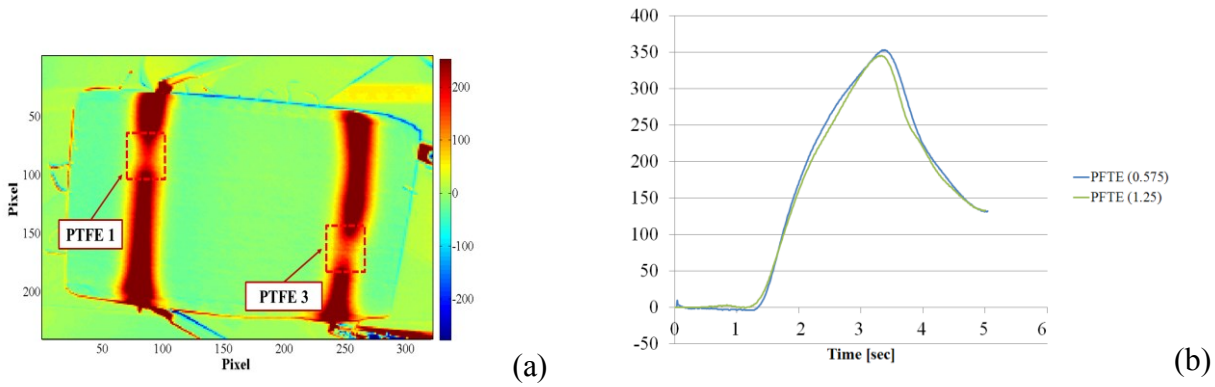

(Figure 12 – a) Thermography images for multiple defective parts of *Sample C* at t=3s; b) Amplitude contrast of apparent temperature variation for PFTE1 (0.575mm) and PFTE3 (1.25)

5. Conclusions

The work presented in this paper investigates a novel in situ approach for the evaluation of health status for advanced composite structures using SMA-embedded composite material. Such a smart material, exploits the unique SMA properties not only to increase the mechanical properties of composite parts, but also to employ them as a strain gauge sensor and damage detection system. The electrical resistance variation and the internal Joule heating source provided by a network of NiTi wires, allowed a quick detection of the material strain distribution, and an *in situ* damage imaging using a step heating thermography process. In order to validate the efficiency of these techniques, several tests were carried on a number of laminates with different configurations. Results clearly show that the strain sensing and damage detection were achieved with high accuracy, without the need to use large external heaters or complex signal processing techniques as the heat source is embedded into the material.

References:

[1] A. Serge, "Modeling of impacts on composite structures," Composite Structures, 51(2), 129-138 (2001).

[2] U. Polimeno, and M. Meo, "Detecting barely visible impact damage detection on aircraft composites structures," Composite Structures, 91(4), 398-402 (2009).

[3] G. Zumpano, and M. Meo, "Damage detection in an aircraft foam sandwich panel using nonlinear elastic wave spectroscopy," Computers & Structures, 86(3–5), 483-490 (2008).

[4] G. Zumpano, and M. Meo, "Damage localization using transient non-linear elastic wave spectroscopy on composite structures," International Journal of Non-Linear Mechanics, 43(3), 217-230 (2008).

[5] G. De Angelis, M. Meo, D. P. Almond *et al.*, "A new technique to detect defect size and depth in composite structures using digital shearography and unconstrained optimization," NDT & E International, 45(1), 91-96 (2012).

[6] Y. Bar-Cohen, "In-service NDE of aerospace structures - emerging technologies and challenges at the ent of the 2nd millennium," NDT.net, 4(9), 1-21 (1999).

[7] E. F. Crawley, and E. H. Anderson, "Detailed Models of Piezoceramic Actuation of Beams," Journal of Intelligent Material Systems and Structures, 1(1), 4-25 (1990).

[8] K. Inpil, J. S. Mark, H. K. Jay *et al.*, "A carbon nanotube strain sensor for structural health monitoring," Smart Materials and Structures, 15(3), 737 (2006).

[9] E. Udd, "Fiber optic smart structures," Proceedings of the IEEE, 84(6), 884-894 (1996).

[10] B. T. Khuri-Yakub, F. L. Degertekin, X. C. Jin *et al.*, "Silicon micromachined ultrasonic transducers." 2, 985-991 vol.2.

[11] L. Kin-tak, L. Hang-yin, and Z. Li-min, "Low velocity impact on shape memory alloy stitched composite plates," Smart Materials and Structures, 13(2), 364 (2004).

[12] L. Kin-tak, "Vibration characteristics of SMA composite beams with different boundary conditions," Materials & Design, 23(8), 741-749 (2002).

[13] M. Meo, E. Antonucci, P. Duclaux *et al.*, "Finite element simulation of low velocity impact on shape memory alloy composite plates," Composite Structures, 71(3–4), 337-342 (2005).

[14] S. L. Angioni, M. Meo, and A. Foreman, "Impact damage resistance and damage suppression properties of shape memory alloys in hybrid composites—a review," Smart Materials and Structures, 20(1), 013001 (2011).
[15] Y. Fu, W. Huang, H. Du *et al.*, "Characterization of TiNi shape-memory alloy thin films for MEMS applications," Surface and Coatings Technology, 145(1–3), 107-112 (2001).
[16] X. Gao, M. Huang, and L. C. Brinson, "A multivariant micromechanical model for SMAs Part 1. Crystallographic issues for single crystal model," International Journal of Plasticity, 16(10–11), 1345-1369 (2000).
[17] C. Di, S. Gangbing, and L. Hongnan, "Modeling of the electrical resistance of shape memory alloy wires," Smart Materials and Structures, 19(5), 055019 (2010).
[18] H. S. Carslaw, and J. C. Jaeger, [Conduction of heat in solids] Clarendon Press, (1959).
[19] M. Carosena, and M. C. Giovanni, "Recent advances in the use of infrared thermography," Measurement Science and Technology, 15(9), R27 (2004).
[20] X. Maldague, F. Galmiche, and A. Ziadi, "Advances in pulsed phase thermography," Infrared Physics and Technology, 43(3), 175-181 (2002).
[21] T. Sakagami, and S. Kubo, "Applications of pulse heating thermography and lock-in thermography to quantitative nondestructive evaluations," Infrared Physics & Technology, 43(3–5), 211-218 (2002).